Talanta 101 (2012) 388–395

Contents lists available at SciVerse ScienceDirect

Talanta

journal homepage: www.elsevier.com/locate/talanta

Facile and tunable fabrication of Fe_3O_4/graphene oxide nanocomposites and their application in the magnetic solid-phase extraction of polycyclic aromatic hydrocarbons from environmental water samples

Qiang Han [a,b], Zonghua Wang [b], Jianfei Xia [b], Sha Chen [a], Xiaoqiong Zhang [a], Mingyu Ding [a,*]

[a] Beijing Key Laboratory for Microanalytical Methods and Instrumentation, Department of Chemistry, Tsinghua University, Beijing 100084, China
[b] Laboratory of Fiber Materials and Modern Textile, the Growing Base for State Key Laboratory, Qingdao University, Shandong 266071, China

ARTICLE INFO

Article history:
Received 11 July 2012
Received in revised form
13 September 2012
Accepted 22 September 2012
Available online 27 September 2012

Keywords:
Fe_3O_4/graphene oxide nanocomposite
Electrostatic self-assembly
Magnetic solid-phase extraction
Polycyclic aromatic hydrocarbons
Environmental water samples

ABSTRACT

An electrostatic self-assembly approach was employed to prepare Fe_3O_4/graphene oxide nanocomposites, and their application in the magnetic solid-phase extraction of polycyclic aromatic hydrocarbons from environmental samples was investigated. With the highly hydrophilic graphene oxide sheets and positively charged surface of the Fe_3O_4 nanoparticles, the nanocomposites were synthesized through electrostatic interaction in aqueous solution. Simultaneously, the different loading amounts of Fe_3O_4 onto the graphene oxide were easily controlled by changing the proportion of the initial precursors. The identity of the hybrid materials was confirmed using transmission electron microscopy, X-ray diffraction, X-ray photoelectron spectroscopy and a vibrating sample magnetometer. Five polycyclic aromatic hydrocarbons were selected as model analytes to validate the extraction performance of the Fe_3O_4/GO nanocomposite as a MSPE sorbent. The excellent adsorption property was attributed to the dominant roles of π–π stacking interaction and hydrophobic interaction. After optimizing the conditions, the results indicated that the recoveries of these compounds were in the range of 76.8–103.2%, with relative standard deviations ranging between 1.7% and 11.7%; the limits of detection were in the range of 0.09–0.19 ng mL^{-1}.

1. Introduction

Graphene, a novel class of carbon-based nanomaterial, has attracted considerable research interests because of its extraordinary electronic, thermal and mechanical properties. This material has prompted tremendous theoretical and experimental efforts worldwide [1] since it was discovered by Geim et al. [2] in 2004. Graphene is a single layer of carbon atoms that are densely packed in a honeycomb crystal lattice, which can be viewed as exfoliated "graphite sheets". Based on the remarkable properties, graphene and its hybrid materials have promising potential applications in many areas, such as molecular probing [3,4], electrochemical sensors [5–8] and nanocomposites [9,10].

Recently, magnetic materials are of considerable interests in material chemistry because of their unique physical properties and outstanding surface chemistry properties. These materials have demonstrated many potential applications in drug delivery [11], catalysis [12], and protein immobilization [13]. Furthermore, an increasing number of studies have been concentrated on adsorption and separation using these materials [14–18], which is the so-called magnetic solid-phase extraction (MSPE). MSPE is a new type of SPE based on the combination of magnetic inorganic material and non-magnetic adsorbent material. By taking advantage of the combined benefits of both the materials, the MSPE technology exhibits excellent adsorption efficiency and rapid separation from the matrix by an external magnetic field, and has recently exhibited significant advantages in separation science. On one hand, the sorbent is dispersed in a sample solution instead of being packed into a SPE cartridge. Magnetic separation based on the superparamagnetic Fe_3O_4 is obviously much more convenient, economic and efficient. On the other hand, rapid mass transfer can be obtained due to the sufficiently large contact area between the sorbents and the analytes, which is beneficial for rapid equilibrium. Consequently, MSPE is widely used in sample pretreatment procedures. The most important component of the MSPE technique is the adsorbent material, which dominates the selectivity and sensitivity of the method. Many types of sorbents have currently been used for MSPE, such as C_{18} [19–21], carbon nanotubes [22–24], and polymer materials [25,26]. Zhang et al. [21] evaluated barium alginate caged Fe_3O_4@C_{18} magnetic nanoparticles for the solid-phase extraction of polycyclic aromatic hydrocarbons and phthalate esters from

* Corresponding author. Tel.: +86 10 62797087; fax: +86 10 62781106.
E-mail address: dingmy@mail.tsinghua.edu.cn (M. Ding).

0039-9140/$ - see front matter © 2012 Elsevier B.V. All rights reserved.
http://dx.doi.org/10.1016/j.talanta.2012.09.046

environmental water samples and obtained reliable results. Gao [17] prepared magnetic one-dimensional polyaniline, which was applied in the magnetic solid-phase extraction of fluoroquinolones from honey samples.

Graphene has also been used as the sorbent in the sample pretreatment procedure because of its ultrahigh specific surface area, superior chemical stability and excellent thermal stability. Liu et al. [27] reported the first application of graphene as a sorbent for SPE and revealed the great potential of graphene in analytical processes. In addition, some researches have been focused on the application of graphene in solid-phase microextraction [28–31]. Recently, graphene hybrid materials have aroused extensive interests because of their excellent performance as well as extensive applications. As one kind of graphene hybrid materials, Fe_3O_4/graphene composites have been used as controlled targeted drug carriers [32], arsenic and dye removal [33,34], magnetic resonance imaging [35], etc. The preparation methods for Fe_3O_4/graphene composites, such as chemical precipitation [32], solvothermal reaction [36], and covalent bonding [37], are generally multistep, hard to control and they also require some rigorous conditions. Previous work [38,39] has shown that electrostatic self-assembly is an effective method for fabricating composites that consist of metal oxides and carbon-based materials. Furthermore, electrostatic self-assembly is an easy method for controlling the reaction and has no obvious influence on the properties of the precursors.

Based on the above considerations, we report a simple strategy for preparing Fe_3O_4/graphene oxide nanocomposites through electrostatic self-assembly. It is well known that graphene oxide (GO) sheets are highly negatively charged when dispersed in aqueous solution as a result of the ionization of the carboxylic acid and phenolic hydroxyl groups on the GO sheets. The nanocomposites can be formed through electrostatic interaction after adding Fe_3O_4 that has a positively charged surface. Furthermore, the feeding ratio is conveniently tunable. The obtained composites can also be dispersed in water due to the retained hydrophilic moieties, which are in favor of adsorption in the MPSE procedure. To examine the feasibility of Fe_3O_4/graphene oxide nanocomposites for the application in MSPE, five polycyclic aromatic hydrocarbons (PAHs) were selected as model compounds. The influences of desorption condition, extraction time and the amounts of the sorbent were optimized. A quick, selective and sensitive MSPE–HPLC-UV analytical method was established.

2. Experimental

2.1. Reagents and materials

All reagents used in the experiment were of analytical reagent grade and used without further purification. Expanded graphite powder (100 mesh) was purchased from the Xinghe Graphite Co. Ltd. (Qingdao, China). Fluoranthene (Flu), pyrene (Pyr), benzo[a]anthracene (BaA), benzo[b]fluoranthene (BaF), and benzo[a]pyrene (BaP) were obtained from TCI chemicals (Shanghai, China).

The five individual stock solutions were prepared at a concentration of 1000 μg mL^{-1} and stored at 4 °C. The working standard solution was prepared by combining aliquots of each individual stock solution and diluting to obtain a desired concentration. Fresh working solutions were prepared daily by appropriate dilution of the stock solutions.

2.2. Instrumental and analytical conditions

Transmission electron microscopy images were obtained using a JEM-2100F transmission electron microscope (JEOL, Japan). The powder X-ray diffraction (XRD) measurements were performed using a D8 Advance X-ray diffractometer (Bruker, Germany) with Cu Kα radiation ($\lambda = 1.5406$ Å). X-ray photoelectron spectroscopy (XPS) data were collected using a PHI-5300 ESCA X-ray photoelectron spectrometer (PHI, America). Magnetization curves were recorded using a 7307 Vibrating Sample Magnetometer (LakeShore, America). Zeta potential measurements were performed using a Zetasizer 3000 (Malvern, UK), and the graphene oxide and Fe_3O_4 samples were diluted to 1 mg mL^{-1} before measurements.

The HPLC-UV analysis was performed on a Labtech LC600 (Labtech, China) system. The separation was conducted on an analytical reversed-phase C_{18} column (Ultimate XB-C_{18}, 5 μm particle diameter, 4.6 mm i.d. × 25 cm long) (Ultimate, USA) at room temperature. The five polycyclic aromatic hydrocarbons were chromatographically separated using the isocratic gradient mobile phase of acetonitrile–water (85/15, v/v) at a flow rate of 1.0 mL min^{-1}. The chromatographic data were acquired at the wavelength of 254 nm, and the injection volume was 20 μL.

2.3. Synthesis of Fe_3O_4/graphene oxide nanocomposites

2.3.1. Synthesis of Fe_3O_4 nanoparticles

Fe_3O_4 nanoparticles were prepared using the modified Massart method via the coprecipitation of a mixture of $FeCl_3 \cdot 6H_2O$ and $FeCl_2 \cdot 4H_2O$. The synthesis procedure is described as follows. $FeCl_3 \cdot 6H_2O$ (3.03 g, 11.2 mmol) and $FeCl_2 \cdot 4H_2O$ (1.13 g, 5.6 mmol) were completely dissolved in 150 mL of deaerated deionized water. The aqueous solution was heated to 50 °C to obtain a clear yellow solution under vigorous agitation. Then, 12.5 mL of ammonia was added dropwise and the reaction was maintained for an additional 30 min. N_2 was used as the protective gas throughout the experiment. After the reaction was complete, the black precipitate was collected by an external magnetic field, followed by washing several times with deionized water and ethanol. Finally, the Fe_3O_4 nanoparticles were dried at 60 °C in an oven under vacuum.

2.3.2. Synthesis of graphite oxide

Graphite oxide was prepared from expanded graphite according to a modified Hummers method. The procedure is briefly described as follows. Sodium nitrate (0.5 g) and potassium permanganate (3 g) were added to 23 mL of 98% sulfuric acid in an ice bath. Expanded graphite powder was slowly added with vigorous agitation, and the rate of addition was carefully controlled to avoid a sudden increase of the temperature. The reaction mixture was maintained at approximately 4 °C in an ice bath for 24 h in a refrigerator. Afterward, the reaction was transferred to a 35 °C oil bath for 30 min. Subsequently, 46 mL of deionized water was gradually added to the reaction mixture and the temperature was increased to 98 °C and kept for 15 min. The expanded graphite in the solution was significantly oxidized and became aureate. Then, 30% H_2O_2 was added dropwise until visible bubbles were generated. Remove the supernatant after laying aside, followed by washing with sufficient hydrochloric acid (5%) and deionized water to remove excess acid. Finally, the material was air-dried under ambient conditions.

2.3.3. Synthesis of tunable water-soluble Fe_3O_4/graphene oxide nanocomposites.

The graphene oxide dispersion (GO, 1 mg mL^{-1}) was prepared by ultrasonicating graphite oxide for 1 h. The modified Fe_3O_4 nanoparticles with a positive surface charge were prepared by dispersing Fe_3O_4 in 1 M HNO_3, which generates a positive charge on the surface of the Fe_3O_4 nanoparticles. Then, a specified amount of the Fe_3O_4 nanoparticles was added to the GO dispersion. After 5 h of vigorous stirring of the mixture to obtain a

homogeneous suspension, the resulting nanocomposites were collected by centrifuging and applying an external magnetic field to remove the unbonded Fe_3O_4 nanoparticles and GO sheets. Finally, the nanocomposites were dried at 60 °C in an oven under vacuum. By changing the feeding weight ratio of Fe_3O_4 to GO, three types of Fe_3O_4/graphene oxide ($m_{Fe_3O_4} : m_{GO} = 1$, 5, and 10; note that the composites were defined as Fe_3O_4/GO-a, Fe_3O_4/GO-b and Fe_3O_4/GO-c, respectively) nanocomposites were synthesized.

2.4. Magnetic solid-phase extraction procedures

The entire extraction procedure using the Fe_3O_4/graphene oxide nanocomposite as a sorbent is shown in Fig. 1. First, 40 mg of sorbent (Fe_3O_4/GO-b nanocomposites) was rinsed in 5 mL methanol and 5 mL deionized water and then dispersed into a 50 mL aqueous sample solution by ultrasonicating to form a homogeneous suspension. Second, the mixture was shaken for 10 min to reach adsorption equilibrium, and then a strong magnet was deposited at the bottom of the beaker to isolate the sorbent from the sample solution. After approximately 3 min, the suspension became limpid and the liquid was decanted. After washing with 5 mL of 10% acetonitrile, the preconcentrated target analytes were eluted from the sorbent with 2 mL of acetonitrile/dichloromethane (4:1) after ultrasonicating for 3 min. 20 μL of the eluate was injected into the HPLC system for analysis.

2.5. Sample preparation

Tap water samples were collected from a water tap in our lab (Beijing, China). River water samples were collected from the Xiaoqing River (Beijing, China). Sea water samples were collected from the coast of Maidao (Qingdao, China). All of the environmental water samples were filtered through 0.45 μm microporous membranes immediately after sampling and stored in a volumetric flask at 4 °C in a refrigerator.

3. Results and discussion

3.1. Synthesis of Fe_3O_4/GO nanocomposites

The Fe_3O_4/GO nanocomposite synthesis procedure is schematically illustrated in Fig. 2. The overall synthetic procedure consists of three steps. First, the 10 nm Fe_3O_4 nanoparticles were synthesized by the modified Massart method and then dispersed in 1 M HNO_3 to obtain the positive surface charge due to the adsorption of H^+, which was confirmed by a zeta-potentiometer (32.01 mV). Second, GO was synthesized by the modified Hummer method and then exfoliated in aqueous solution. The surface of the as-prepared GO sheets are highly negatively charged, which is apparently a result of ionization of the carboxylic acid and phenolic hydroxyl groups that are known to exist on the GO

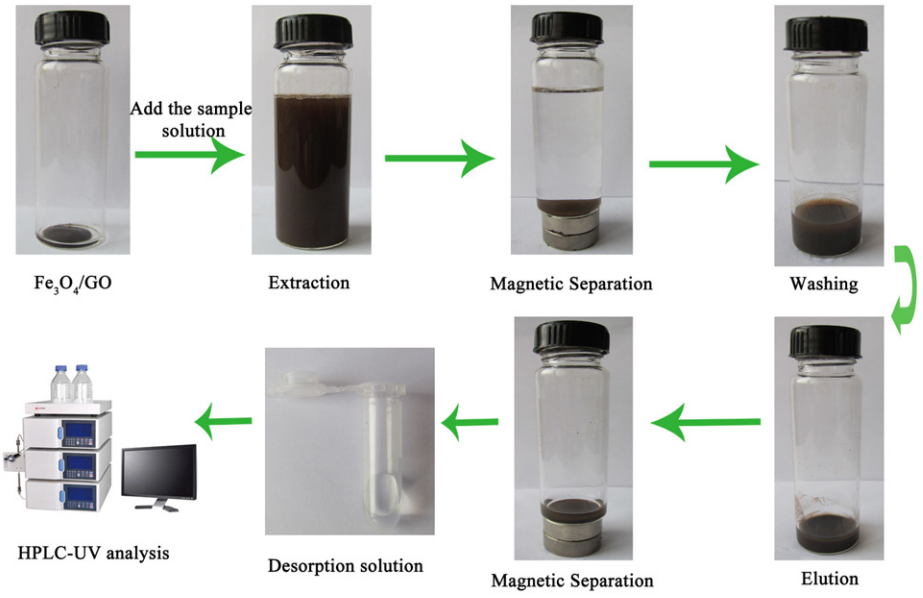

Fig. 1. Experimental magnetic solid-phase extraction procedure using the Fe_3O_4/GO-b nanocomposite.

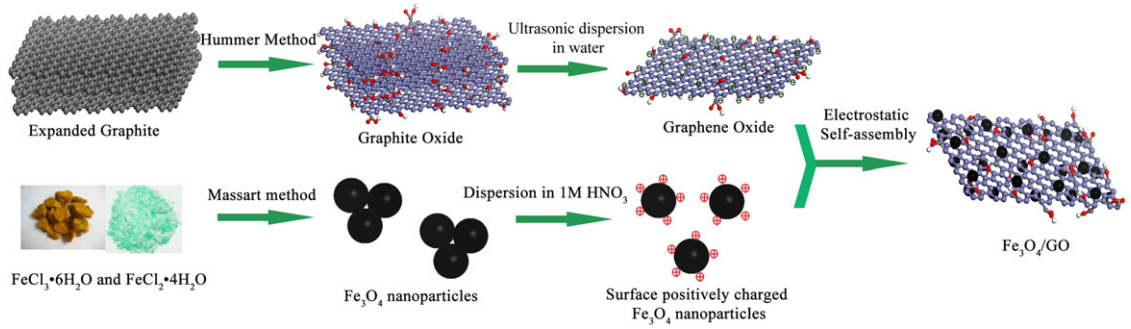

Fig. 2. Schematic illustration of the fabrication of the Fe_3O_4/GO nanocomposite.

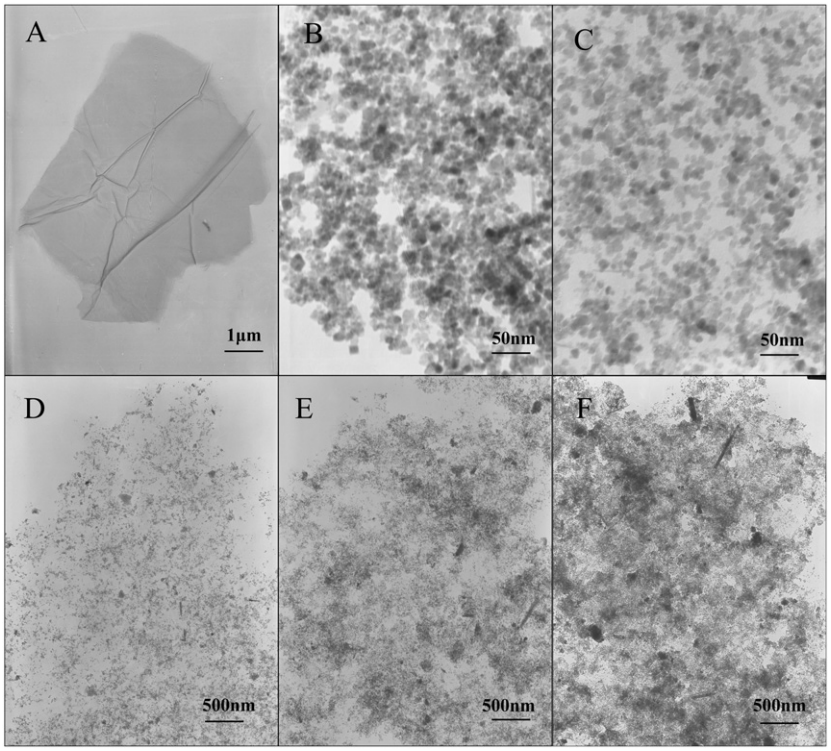

Fig. 3. TEM images of (A) GO, (B) Fe_3O_4, (C) Fe_3O_4/GO-b at magnification, (D) Fe_3O_4/GO-a, (E) Fe_3O_4/GO-b and (F) Fe_3O_4/GO-c.

sheets. The zeta potential of the 1 mg mL^{-1} GO dispersion was −34.93 mV. Third, the surface positively charged Fe_3O_4 nanoparticles were then assembled with the negatively charged GO sheets by electrostatic interaction at room temperature. The complete procedure is mild, green and fast.

In addition, the prepared composite was hydrophilic and easily dispersed in aqueous solution. The composite provided favorable conditions for the following MSPE procedure.

3.2. Characterization of the Fe_3O_4/GO nanocomposites

3.2.1. Transmission electron microscopy

The morphology of the prepared Fe_3O_4 nanoparticles, graphene oxide and Fe_3O_4/GO nanocomposites were characterized by transmission electron microscopy (TEM). As shown in Fig. 3B, the TEM image of Fe_3O_4 revealed that the obtained gray nanoparticles were spherical in shape with a mean diameter of approximately 10 nm, and they aggregated because of their extremely small size and dipole–dipole coupling. The GO sheet exhibited an irregular shape and contained some wrinkles, which maintained a large surface area (Fig. 3A). Fig. 3D–F present the representative TEM images of the obtained Fe_3O_4/GO nanocomposites with different Fe_3O_4 loading amounts. It can be observed that the Fe_3O_4 nanoparticles were homogeneously anchored onto the surface of the GO sheets, although the pristine Fe_3O_4 nanoparticles were aggregated. This observation was attributed to electrostatic self-assembly between the positively charged surface of the Fe_3O_4 and the negatively charged GO in aqueous solution, which also decreases the possibility of serious agglomeration and restacking of the GO sheets. Furthermore, the loading amounts in the composites were effectively controlled by changing the feeding mass ratio of Fe_3O_4 to GO. Fig. 3C presents the TEM image of the Fe_3O_4/GO-b at magnification. The diameter of the Fe_3O_4 nanoparticle on the GO sheet was the same as the pristine Fe_3O_4, which is also evidence of the electrostatic self-assembly.

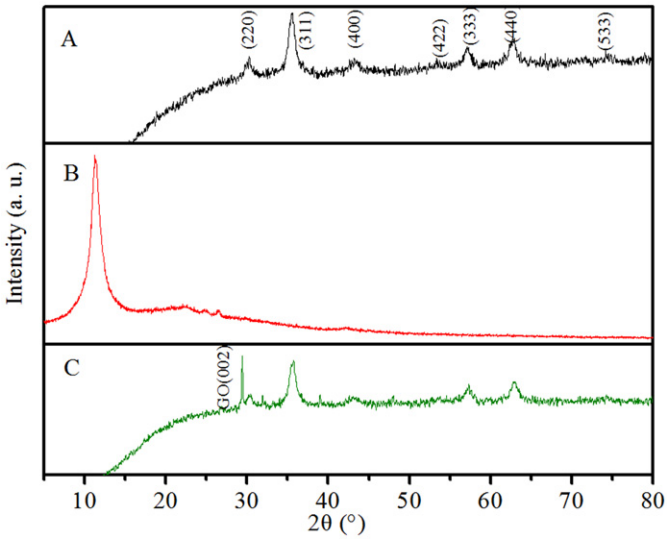

Fig. 4. XRD patterns of (A) Fe_3O_4, (B) graphite oxide and (C) Fe_3O_4/GO-b.

3.2.2. X-ray diffraction

As shown in Fig. 4, X-ray diffraction (XRD) measurements were performed to obtain crystalline structural information for the as-synthesized Fe_3O_4, graphite oxide and Fe_3O_4/GO-b. The position and relative intensities of all diffraction peak at 2θ=30.25°, 35.58°, 43.21°, 54.39°, 57.09°, 62.92° and 75.19° can be assigned to the (220), (311), (400), (422), (511), (440), and (533) reflections, respectively, so the pure cubic spinel crystal structure of Fe_3O_4 is confirmed (Fig. 4A). The graphite oxide (Fig. 4B) presents a very sharp diffraction peak at 2θ=11.28°, which indicates that the (002) inter-planar spacing increased due to the oxide treatment, whereas the weak wide peak at 2θ=22.68° suggests residual unoxidized graphite. When the Fe_3O_4/GO-b (Fig. 4C)

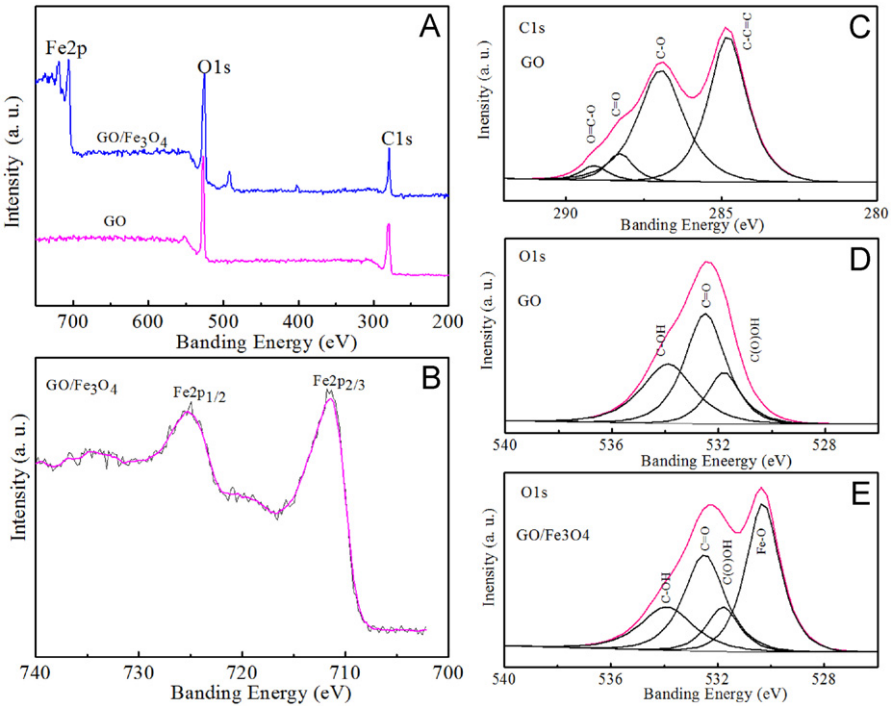

Fig. 5. XPS spectra of (A) wide scan of GO and Fe_3O_4/GO-b, (B) Fe 2p spectrum, (C) C1s spectrum, (D) O1s spectrum of Fe_3O_4 and (E) O1s spectra of Fe_3O_4/GO-b.

was generated, the characteristic peak of Fe_3O_4 remained unchanged, but the diffraction peak for graphene oxide increased to $2\theta = 29.42^{\circ}$, which indicated the formation of graphene oxide from graphite oxide after ultrasonicating. Furthermore, the diffraction pattern confirmed the formation of the Fe_3O_4/GO nanocomposites.

3.2.3. X-ray photoelectron spectroscopy

X-ray photoelectron spectroscopy (XPS) was used to determine the chemical composition of the Fe_3O_4/GO composites. The wide scan XPS spectra (Fig. 5A) of the GO and Fe_3O_4/GO-b exhibited the same photoelectron lines at binding energies of approximately 280 and 520 eV, which were attributed to C1s and O1s, respectively. However, the sharp peaks approximately 710 eV, which correspond to the characteristic peaks of Fe 2p in Fe_3O_4/GO-b, indicated the existence of carbon, oxygen, and iron in the composite. In the Fe 2p spectrum (Fig. 5B), the peaks at 711.29 and 724.82 eV, which correspond to the Fe $2p_{1/2}$ and Fe $2p_{3/2}$ spin–orbit peaks of Fe_3O_4, indicated the formation of the Fe_3O_4 phase in the composites. Fig. 5C illustrates the C1s deconvolution spectrum of GO, and four different oxygen containing functional groups of (a) the non-oxygenated carbon (–C═C) at 284.8 eV, (b) the epoxyl and alkoxyl carbon (C–O) at 286.9 eV, (c) the carbonyl carbon (C═O) at 288.2eV, and (d) the carboxylate carbon (O–C═O) at 289.0 eV were observed, which indicated successful oxidation of the expanded graphite. Three peaks were present in the O1s spectrum of GO (Fig. 5D), which corresponded to C(O)OH at 531.8 eV, C═O at 532.5 eV and C-OH at 533.9 eV. The discrepancy was the peak at 530.2 eV in the O1s spectra of Fe_3O_4/GO-b (Fig. 5E), which was the contribution of the anionic oxygen in Fe_3O_4.

3.2.4. Vibrating sample magnetometer

The magnetic properties of the Fe_3O_4 and the Fe_3O_4/GO nanocomposites with different loading amounts were determined using a superconducting quantum interference device (SQUID) at room temperature by cycling the field between −20 and 20 kOe (Fig. 6). The magnetization hysteresis loops of all of the

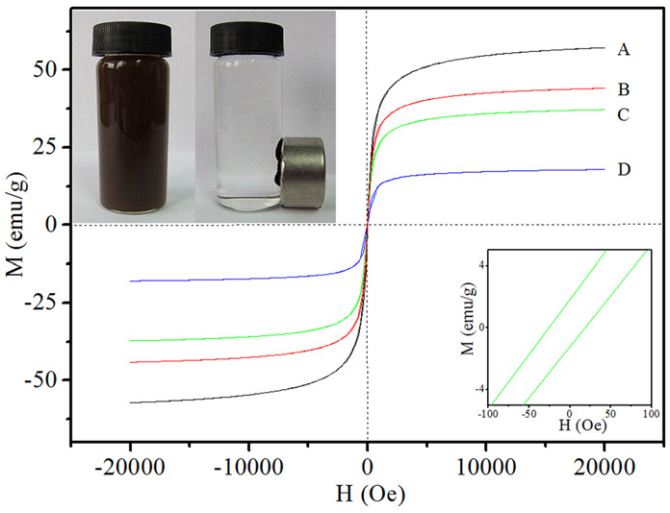

Fig. 6. The magnetization hysteresis loops of (A) Fe_3O_4, (B) Fe_3O_4/GO-a, (C) Fe_3O_4/GO-b and (D) Fe_3O_4/GO-c.

composites were S-like curves, which indicated that the composites were superparamagnetic. The specific saturation magnetization (M_s) of the composites (Fe_3O_4/GO-a, Fe_3O_4/GO-b and Fe_3O_4/GO-c) were 17.9, 37.2 and 44.1 emu g^{-1}, respectively, which increased with the increased loading amounts of Fe_3O_4. However, small remnant magnetization and coercivity were present at room temperature (the graph is shown in the bottom right inset of Fig. 6), but it was negligible in the practical application. A total of 10 mL of a 1 mg/mL GO/Fe_3O_4-b aqueous dispersion was rapidly separated under an external magnetic field (the graph is shown in the top left inset of Fig. 6).

3.3. Optimization of the MSPE conditions

The feeding weight ratio of Fe_3O_4 anchored on the surface of graphene oxide is very important in the following analytical

procedure. A higher feeding weight will enhance the magnetic properties of Fe_3O_4/GO, and it can easily be separated in aqueous solution under an external magnetic field within a short time. However, a high feeding weight will decrease the exposed surface area of GO, and it not only reduces the dispersion of the composite in aqueous solution but also results in a lower adsorption capacity for the analytes. In order to investigate the adsorptive capabilities of Fe_3O_4/GO for PAHs, 10 mg of the three kinds of nanocomposites were added into 50 mL aqueous solution containing each analyte at 10 μg mL^{-1} level. The adsorptive capacities (q_e in mg g^{-1}) of Fe_3O_4/GO were calculated according to the following equation:

$$q_e = \frac{(C_0 - C_e)V}{m}$$

where C_0 and C_e represent the initial and equilibrium concentrations of the analyte in aqueous solution (mg L^{-1}), V is the volume of the solution (L), and m is the mass of the adsorbent (g). The results showed that the values of q_e for the composites are: Fe_3O_4/GO-a > Fe_3O_4/GO-b > Fe_3O_4/GO-c. They increased with the proportion of GO in the composites which indicated that GO played an important role in the extraction procedure. We investigated the feasibilities of the three composites in the MSPE step. The adsorptive capability of Fe_3O_4/GO-c is much smaller (lower than 20 mg g^{-1} for all the analytes), and the specific saturation magnetization of Fe_3O_4/GO-a is so small that it requires much more time for the separation from aqueous solution. The q_e of the Fe_3O_4/GO-b composite is higher than 40 mg g^{-1} for all the analytes. It is sufficient for the extraction of trace contamination from large volume samples. It is known that high sample loading volume can give rise to high concentration factors. However, it might lead to poor recoveries. In addition, high sample loading volume in MSPE would greatly extend magnetic separation time. The Fe_3O_4/GO-b composite can be separated from 50 mL aqueous solution in 3 min, but it required nearly 30 min for the separation from 100 mL aqueous solution. It was a waste of time. Therefore, the Fe_3O_4/GO-b composite and 50 mL volume sample were selected for the following investigation.

To select the optimal MSPE conditions for extracting the PAHs, 50 mL of deionized water spiked with 5 μg L^{-1} of each of the five PAHs was used to examine the extraction performance of the MSPE under different experimental conditions. In our experiments, several parameters, including the desorption condition, extraction time, sample pH, ionic strength and the amounts of the sorbent were investigated to achieve the best extraction efficiency for PAHs.

3.3.1. *Effect of the desorption condition for PAHs*

It is necessary to choose an effective elution to achieve higher recovery, therefore, the choice of elution solvent should be carefully considered. In this study, four different organic solvents were studied to elute PAHs from the Fe_3O_4/GO-b composites. In each case, the sorbents were loaded with 0.25 μg of each PAH in aqueous solution. After sufficient extraction time, 2 mL of different eluents were used to desorb the five analytes. The obtained peak area is shown in Fig. 7. As shown, acetonitrile had a higher desorption capacity toward all of the PAHs compared to methanol and acetone. However, all of the three solvents were scantly eluted toward the higher number of condensed ring PAHs because the π–π stacking interaction between the sorbents and the analytes is increasing with the ring number of PAHs. Li et al. [40] reported that dichloromethane had a satisfactory recovery for higher molecular weight PAHs. However, the prepared Fe_3O_4/GO composite was hydrophilic, and its dispersive capacity in nonpolar solvents such as dichloromethane was poor. In this work, the mixed solution of acetonitrile and dichloromethane with different ratios (1:1; 2:1; 4;1; 8:1 v/v) were tested as the elution solutions. The results showed that high proportion of dichloromethane also caused poor dispersion of the sorbent, and the elution capacity of 4:1 (v/v) mixed solution of acetonitrile and dichloromethane was higher than 8:1 (v/v) mixed solution of acetonitrile and dichloromethane. Therefore, a mixed eluent of acetonitrile and dichloromethane (4:1 v/v) was used as the eluent.

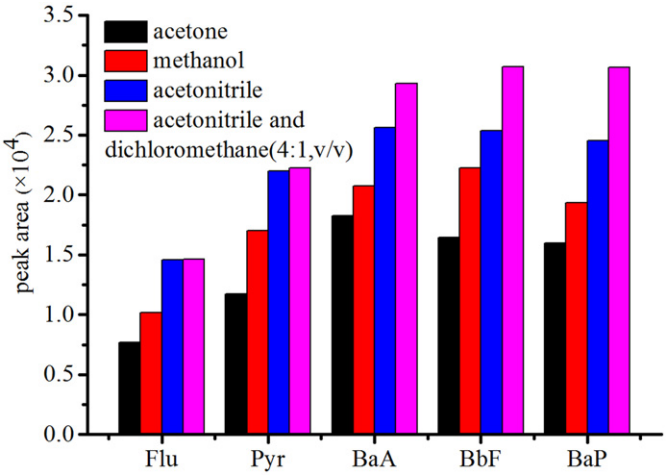

Fig. 7. The effect of desorption solvents on the extraction efficiency of PAHs.

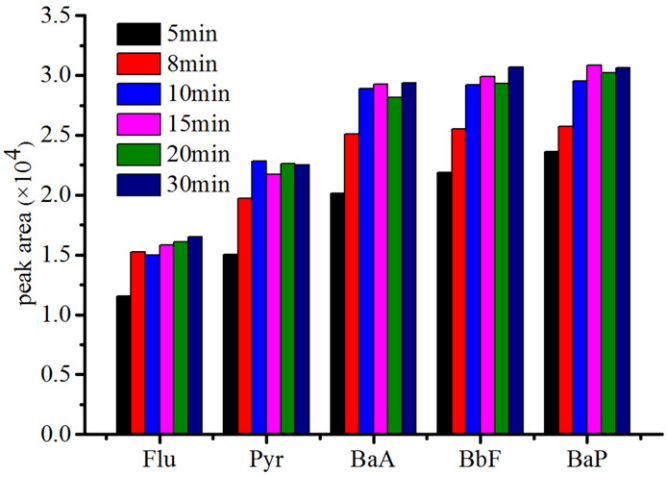

Fig. 8. The effect of extraction time on the extraction efficiency of PAHs.

3.3.2. *Effect of the extraction time*

The extraction time profiles were studied by varying the absorption time between 5 and 30 min. As shown in Fig. 8, the peak area reached a maximum for Flu at 8 min, and for Pyr, BaA, BbP and BaP at 10 min. It can be concluded that extraction equilibrium between the aqueous phases and the sorbents was nearly reached after 10 min. Hence, an extraction time of 10 min was chosen for the subsequent experiments.

3.3.3. *Effect of the pH and Ionic strength*

The pH of the solution plays an important role for the sorbent to target analytes. pH not only changes the formation of the analytes but also alters the interaction between the sorbents and the analytes. The solution pH will change the charge property of the surface of Fe_3O_4/GO, which is a primary factor that affects the adsorption property towards the analytes. In our experiment, the

influence of the sample pH on the extraction efficiency was investigated by adjusting the pH in the range of 3–10 by adding appropriate volumes of 1 M NaOH or 1 M HCl. No obvious variations in the peak areas of PAHs were observed. PAHs exist as neutral molecules under ordinary conditions, and their formation was maintained invariably when the pH changed. Therefore, there is no need to adjust the sample pH.

To investigate the effect of ionic strength on the extraction efficiency of PAHs, NaCl was added to adjust the ionic strength of the solution. No significant variation in the extraction efficiency was observed with the NaCl concentration between 0 and 100 mM. This result indicated that the ionic strength was negligible for the next analytical procedure.

3.3.4. Effect of the amounts of the sorbent

The effect of dosage of the Fe_3O_4/GO-b on the extraction efficiency of the PAHs from spiked aqueous samples is presented in Fig. 9. The peak areas increased with increasing sorbent doses from 20 to 40 mg, and then stabilized with further increases. This result indicated that 40 mg of sorbent was sufficient to extract PAHs from 50 mL of an aqueous sample. In the following experiments, 40 mg of the Fe_3O_4/GO-b nanocomposite was used to ensure the complete adsorption of the analytes.

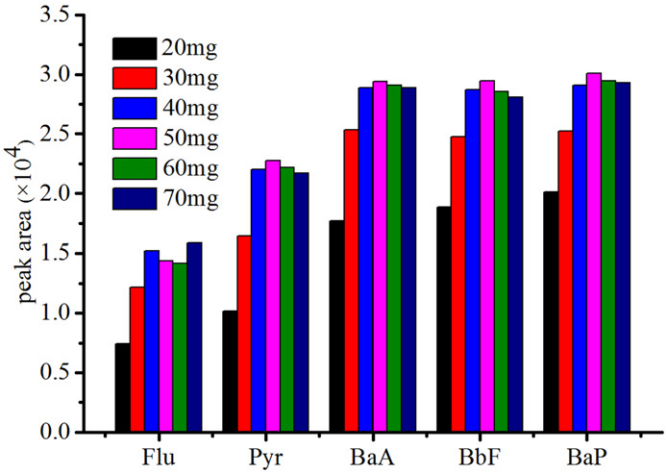

Fig. 9. The effect of the amounts of the sorbent on the extraction efficiency of PAHs.

Table 1
Parameters of the proposed method for quantitative analysis (n=5).

Analyte	Linear range (ng mL^{-1})	Regression equation	R^2	RSD (%)	LOD (ng mL^{-1})
Flu	0.5–100	y=3177+2465x	0.9965	2.9	0.19
Pyr	0.5–100	y=10219+2584x	0.9943	3.7	0.12
BaA	0.5–100	y=9146+4288x	0.9993	2.6	0.09
BbF	0.5–100	y=13070+3544x	0.9956	3.5	0.10
BaP	0.5–100	y=12793+3475x	0.9830	4.5	0.13

3.4. Validation of the HPLC coupled with the proposed MSPE method

Under the optimized conditions, a series of quantitative parameters with regard to the linear range, correlation coefficient, limit of detection (LOD), and reproducibility were examined to validate the proposed MSPE–HPLC method. Linear regression analysis was performed using the peak areas against the concentrations of the respective analytes. The LODs were calculated as a signal-to-noise ratio of three.The precision of the MSPE–HPLC method was assessed by five parallel extractions of each analyte (10 ng mL^{-1}). As listed in Table 1, all of the analytes exhibited good linearity with satisfactory regression coefficients (R^2=0.9830–0.9993). The LODs were determined to range from 0.09 to 0.19 ng mL^{-1}. The present method was compared with other previous extraction methods that were used for the determination of PAHs [41–45], the results are summarized in Table 2. The present method required smaller amounts of the sorbent, or conveniently manipulation, but exhibited better performations.

3.5. Analysis of environmental water samples

The environmental influences of polycyclic aromatic hydrocarbons have attracted global attention because of their potential carcinogenic and mutagenic properties. Because of the low concentration in environmental water samples, the common analytical methods for analyzing PAHs are GC–MS [45,46] and HPLC–ESI–MS [47]. However, these methods are somewhat complex and costly. In our study, PAHs were analyzed using a universal HPLC-UV and the proposed MSPE method to preconcentrate the samples.

The MSPE–HPLC method developed in this work was used to analyze several environmental water samples, including tap water, river water and sea water. To estimate the influence of the matrix,

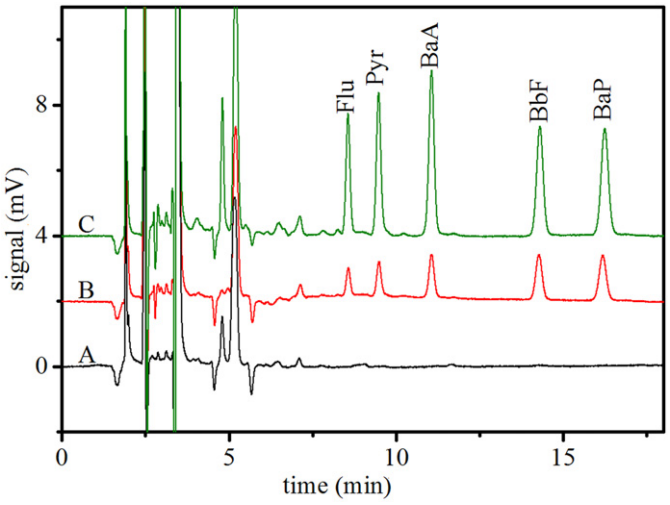

Fig. 10. The typical chromatograms of sea water sample (A) and its corresponding spiked samples with (B) 1 ng mL^{-1} and (C) 10 ng mL^{-1} of each analyte.

Table 2
Comparison of different methods for PAHs extraction.

Method	Detection	Amount of sorbent (mg)	Sample volume (mL)	LODs (ng mL^{-1})	Refs.
Multiwalled carbon nanotubes based SPE	HPLC-UV	200	100	0.005–0.058	[41]
Headspace solvent microextraction	GC-FID	-	0.003	4–41	[42]
Microwave assisted headspace solid-phase microextraction	GC-FID	-	20	0.03–1.0	[43]
Carbon-ferromagnetic nanocomposites based MSPE	GC–MS	10	20	0.015–0.335	[44]
C18/Fe_3O_4 based MSPE	GC–MS	50	20	0.8–36	[45]
Fe_3O_4/GO based MSPE	HPLC-UV	40	50	0.09–0.19	This work

Table 3
Recoveries of real water samples spiked with five target analytes (n=3).

Analyte	Concentration added (ng mL^{-1})	Tap water samples		River water samples		Sea water samples	
		Recovery (%)	RSD (%)	Recovery (%)	RSD (%)	Recovery (%)	RSD (%)
Flu	1	92.3	5.6	100.3	11.7	83.8	3.6
	10	87.6	3.1	86.2	2.3	94.3	3.8
Pyr	1	89.7	5.2	87.3	10.2	84.7	6.7
	10	93.3	2.9	101.2	4.3	99.6	3.0
BaA	1	86.3	8.4	76.8	8.7	80.9	2.3
	10	100.9	3.2	89.2	2.9	97.7	1.7
BbF	1	78.6	7.9	83.4	9.22	93.8	3.2
	10	89.5	4.9	88.6	6.4	88.1	3.7
BaP	1	103.2	3.0	86.0	9.5	89.4	3.8
	10	94.2	4.6	97.2	5.4	99.1	2.9

all of the samples were spiked with different concentrations of analytes to determine the recovery of the targeted analytes. Fig. 10 presents typical chromatograms obtained from unspiked water samples and from water samples spiked with different concentration levels of the analytes. As shown in Table 3, satisfactory recoveries, ranging from 76.8% to 101.2%, were observed for the environmental water samples.

4. Conclusions

A simple electrostatic self-assembly method has been developed to fabricate tunable Fe_3O_4/graphene oxide nanocomposites. The synthesis procedure is mild, fast and does not use toxic reagents. The obtained hybrid materials were used as a MSPE sorbent to preconcentrate several polycyclic aromatic hydrocarbons in environmental water samples before HPLC-UV detection. The extraction was very fast, and the sorbent was easily separated from the sample solution. Satisfactory recoveries were attained for the real environmental water samples. The results indicated that the developed method can be used as a simple and efficient extraction and preconcentration technique for trace PAHs in water samples.

Acknowledgments

This project was supported by the National Nature Science Foundation of China (No. 21075074).

References

[1] A.K. Geim, K.S. Novoselov, Nat. Mater. 6 (2007) 183–191.
[2] K.S. Novoselov, A.K. Geim, S.V. Morozov, D. Jiang, Y. Zhang, S.V. Dubonos, I.V. Grigorieva, A.A. Firsov, Science 36 (2004) 666–669.
[3] Y. Wang, Z.H. Li, D.H. Hu, C.T. Lin, J.H. Li, Y.H. Lin, J. Am. Chem. Soc. 132 (2010) 9274–9276.
[4] L. Lin, Y. Liu, X. Zhao, J.H. Li, Anal. Chem. 83 (2011) 8396–8402.
[5] L.H. Tang, Y. Wang, Y.M. Li, H.B. Feng, J. Lu, J.H. Li, Adv. Funct. Mater. 19 (2009) 2782–2789.
[6] Y. Wang, Y.Y. Shao, D.W. Matson, J.H. Li, Y.H. Lin, ACS Nano 4 (2010) 1790–1798.
[7] Z.H. Wang, J.F. Xia, L.Y. Zhu, X.Y. Chen, F.F. Zhang, S.Y. Yao, Y.H. Li, Y.Z. Xia, Electroanalysis 23 (2012) 2463–2471.
[8] Z.H. Wang, J.F. Xia, L.Y. Zhu, F.F. Zhang, X.M. Guo, Y.H. Li, Y.Z. Xia, Sens. Actuators B: Chem. 161 (2012) 131–136.
[9] X.L. Wang, H. Bai, Z.Y. Yao, A.R. Liu, G.Q. Shi, J. Mater. Chem. 20 (2010) 9032–9036.
[10] X.L. Wang, H. Bai, Y.Y. Jia, L.J. Zhi, L.T. Qu, Y.X. Xu, C. Li, G.Q. Shi, RSC Adv. 2 (2012) 2154–2160.
[11] X.L. Li, H. Li, G.Q. Liu, Z.W. Deng, S.L. Wu, P.H. Li, Z.S. Xu, H.B. Xu, Paul K. Chu, Biomaterials 33 (2012) 3013–3024.
[12] M. Feyen, C. Weidenthaler, F. Schüth, A.H. Lu, Chem. Mater. 22 (2011) 2955–2961.
[13] B. Teste, J. Vial, S. Descroix, T. Georgelin, J.M. Siaugue, J. Petrc, A. Varennec, M.C. Henniona, Talanta 81 (2010) 1703–1710.
[14] R. Fuhrer, I.K. Herrmann, E.K. Athanassiou, R.N. Grass, W.J. Stark, Langmuir 27 (2011) 1924–1929.
[15] H.M. Jiang, Z.P. Yan, Y. Zhao, X. Hu, H.Z. Lian, Talanta 94 (2012) 251–256.
[16] X.Y. Liu, J.J. Yin, L. Zhu, G.H. Zhao, H.X. Zhang, Talanta 85 (2011) 2451–2457.
[17] Q. Gao, H.B. Zheng, D. Luo, J. Ding, Y.Q. Feng, Anal. Chim. Acta 720 (2012) 57–62.
[18] Y.Y. Geng, M.Y. Ding, H. Chen, H.F. Li, J.M. Lin, Talanta 89 (2012) 189–194.
[19] X.L. Zhang, H.Y. Niu, Y.Y. Pan, Y.L. Shi, Y.Q. Cai, Anal. Chem. 82 (2010) 2363–2371.
[20] Y.F. Sha, C.H. Deng, B.Z. Liu, J. Chromatogr. A 1198–1199 (2008) 27–33.
[21] S.X. Zhang, H.Y. Niu, Y.Q. Cai, Y.L. Shi, Anal. Chim. Acta 665 (2010) 167–175.
[22] Q. Zhao, F. Wei, Y.B. Luo, J. Ding, N. Xiao, Y.Q. Feng, J. Agric. Food Chem. 59 (2011) 12794–12800.
[23] Y.B. Luo, Q.W. Yu, B.F. Yuan, Y.Q. Feng, Talanta 90 (2012) 123–131.
[24] B. Chen, S. Wang, Q.M. Zhang, Y.M. Huang, Analyst 137 (2012) 1232–1240.
[25] Q. Gao, D. Luo, J. Ding, Y.Q. Feng, J. Chromatogr. A 1217 (2010) 5602–5609.
[26] Q. Gao, D. Luo, M. Bai, Z.W. Chen, Y.Q. Feng, J. Agric. Food Chem. 59 (2011) 8543–8549.
[27] Q. Liu, J.B. Shi, L.X. Zeng, T. Wang, Y.Q. Cai, G.B. Jiang, J. Chromatogr. A 1218 (2011) 197–204.
[28] J.M. Chen, J. Zou, J.B. Zeng, X.H. Song, J.J. Ji, Y.R. Wang, J. Ha, X. Chen, Anal. Chim. Acta 678 (2010) 44–49.
[29] S.L. Zhang, Z. Du, G.K. Li, Anal. Chem. 83 (2011) 7531–7541.
[30] H. Zhang, H.K. Lee, J. Chromatogr. A 1218 (2011) 4509–4516.
[31] V.K. Ponnusamy, J.F. Jen, J. Chromatogr. A 1218 (2011) 6861–6868.
[32] X.Y. Yang, X.Y. Zhang, Y.F. Ma, Y. Huang, Y.S. Wang, Y.S. Chen, J. Mater. Chem. 19 (2009) 2710–2714.
[33] V. Chandra, J. Park, Y. Chun, J.W. Lee, I.-C. Hwang, K.S. Kim, ACS Nano 4 (2010) 3979–3986.
[34] H.M. Sun, L.Y. Cao, L.H. Lu, Nano Res. 4 (2011) 550–562.
[35] H.P. Cong, J.J. He, Y. Lu, S.H. Yu, Small 6 (2010) 169–173.
[36] K.F. Zhou, Y.H. Zhu, X.L. Yang, C.Z. Li, New J. Chem. 34 (2010) 2950–2955.
[37] F. He, J.T. Fan, D. Ma, L.M. Zhang, C. Leung, H.L. Chan, Carbon 48 (2010) 3139–3144.
[38] F. Stoffelbach, A. Aqil, C. Jerome, R. Jerome, C. Detrembleur, Chem. Commun. (2005) 4532–4533.
[39] W.L. Zhang, H.J. Choi, Chem. Commun. 47 (2011) 12286–12288.
[40] K. Li, H.F. Li, L.B. Liu, Y. Hashi, T. Maedac, J.M. Lin, J. Chromatogr. A 1154 (2007) 74–80.
[41] W.D. Wang, Y.M. Huang, W.Q. Shu, J. Cao, J. Chromatogr. A 1173 (2007) 27–36.
[42] S.S. Feizabadi, Y. Yamini, N. Bahramifar, Anal. Chim. Acta 489 (2003) 21–31.
[43] M.C. Wei, J.F. Jen, Talanta 72 (2007) 1269–1274.
[44] L. Bai, B. Mei, Q.Z. Guo, Z.G. Shi, Y.Q. Feng, J. Chromatogr. A 1217 (2010) 7331–7336.
[45] Y. Liu, H.F. Li, J.M. Lin, Talanta 77 (2009) 1037–1042.
[46] J.P. Ma, R.H. Xiao, J.H. Li, J.B. Yu, Y.Q. Zhang, L.X. Chen, J. Chromatogr. A 1217 (2010) 5462–5469.
[47] M. Takino, S. Daishima, K. Yamaguchi, T. Nakahara, J. Chromatogr. A 928 (2001) 53–61.